Effects of Streambed Morphology and Biofilm Growth on the Transient Storage of Solutes

ANDREA BOTTACIN-BUSOLIN,*,† GABRIEL SINGER,‡ MATTIA ZARAMELLA,† TOM J. BATTIN,‡ AND ANDREA MARION†

Department of Hydraulic, Maritime, Environmental and Geotechnical Engineering, University of Padova, Via Loredan 20, I-35131, Padova, Italy, Department of Freshwater Ecology, University of Vienna, Althanstrasse 14, A-1090 Vienna, Austria, and WasserKluster Lunz GmbH, 3293 Lunz am See, Austria

Received March 21, 2009. Revised manuscript received July 16, 2009. Accepted August 18, 2009.

Microbial biofilms are the prime site of nutrient and contaminant removal in streams. It is therefore essential to understand how biofilms affect hydrodynamic exchange, solute transport, and retention in systems where geomorphology and induced hydrodynamics shape their growth and structure. We experimented with large-scale streamside flumes with streambed landscapes constructed from graded bedforms of constant height and wavelength. Each flume had a different bedform height and was covered with a layer of gravel as substratum for benthic microbial biofilms. Biofilms developed different biomass and physical structures in response to the hydrodynamic conditions induced by the streambed morphology. Step injections of conservative tracers were performed at different biofilm growth stages. The experimental breakthrough curves were analyzed with the STIR model, using a residence time approach to characterize the retention effects associated with biofilms. The retained mass of the solute increased with biofilm biomass and the biofilm-associated retention was furthermore related to bedform height. We tentatively relate this behavior to biofilm structural differentiation induced by bed morphology, which highlights the strong linkage between geomorphology, hydrodynamics, and biofilms in natural streams and provide important clues for stream restoration.

Introduction

Transient storage in natural streams receives increasing attention because of its implications in contaminant, nutrient, pathogens, and particle retention. Studies on solute retention at the streambed-streamwater interface (i.e., the hyporheic zone) (*1*−*6*) have highlighted the role of sediment heterogeneity (*7, 8*) and planimetric induced hyporheic fluxes (*9*−*11*) for transient storage. Collectively, they show that transient storage involves complex processes acting simultaneously over a wide range of spatial and temporal scales, from microbial biofilms to entire catchments.

In streams, microbial life is often dominated by biofilms (matrix-enclosed communities including bacteria, archaea, algae, fungi, and protozoa) coating the sediments (*12*). Understanding the controls of biofilms on solute transport is essential given the contributions of streams to biogeochemical fluxes (*13, 14*). Biofilms differentiate into complex physical structures such as filamentous streamers floating in the water and thereby adapt to the hydrodynamic conditions (*15*). Biofilm differentiation also results from interactions between mass transport, conversion, shear-induced erosion, and compacting (*15*). Ultimately, this differentiation can create retention domains at the streambed−streamwater interface, which can act as solute storage zones in support of biological activity as shown in a range of studies. For instance, Kim et al. (*16, 17*) simulated nitrate retention by periphytic (i.e., phototrophic) biofilms based on hydrologic advection−dispersion transport, transient storage (*18*), and Michaelis−Menten uptake kinetics. Mulholland et al. (*19*) used an advection−dispersion model to show how dispersion coefficients and transient storage zones increase with periphytic biomass. DeAngelis et al. (*20*) showed the effect of periphytic biofilms on stream hydraulics using a single storage zone model, which was then extended to include hyporheic exchange as a separate retention domain to consider the effect of periphyton on subsurface nitrogen cycling (*21*). Gooseff et al. (*22*) attributed rapid nitrate removal to the transient storage zone created by periphytic mats rather than to the hyporheic zone. Recently, Orr et al. (*23*) reported hyporheic processes to dominate nutrient retention when periphytic biomass is low, whereas nutrient retention became allocated to the benthic zone as biomass developed and clogged the sediments.

In this study, we experimented with streamside flumes with low submergence-streambeds to evaluate how solute transient storage is mutually affected by bed morphology and related biofilm. Illuminating this link is important to help restore headwater streams. Our analysis is based on the theoretical framework of the STIR (solute transport in rivers) model (*24, 25*), which allows for general residence time modeling of processes acting at different temporal and spatial scales. The determination of model parameters and of the mass retained allowed us to separate effects of biofilms and bed-induced hydrodynamics.

Experimental Methods

We constructed streambeds in five streamside flumes (length, 40 m; width, 0.4 m; Lunz am See, Austria). The bottom of each flume was shaped from impermeable bedforms (wavelength $L = 1$ m, horizontal distance between the crest and the upstream trough $L_c = 0.75$ m, and height $H = 2$, 4, 6, 8, 10 cm, respectively) (Figure S1, Supporting Information). Bedforms were covered with a single layer of indigenous, clean, and graded (median grain diameter, 9.2 mm) sediment as substratum for biofilm growth (Figure S2, Supporting Information). This setup with limited size of hyporheic storage zones simulated stream reaches with bedrock and constrained hyporheic zones. All flumes were continuously fed from the same header tank with raw streamwater (Oberer Seebach) in a once-through mode to ensure identical water chemistry and microbial inoculum. Periodically measured concentrations of NO_3−N, NH_4−N and dissolved organic carbon (DOC) averaged 0.57 ± 0.24 mg L^{-1} (mean ± standard deviation, $n = 22$), 4.4 ± 4.25 μg L^{-1} ($n = 24$), and 1.49 ± 0.52 mg L^{-1} ($n = 39$), respectively. Concentrations of PO_4−P were mostly below the detection limit (<3 μg L^{-1}). Water temperature averaged 9.1 ± 1.3 °C. The flow rate was adjusted to 2.25 ± 0.10 L s^{-1} by fixing the water level in the header tank and checked daily throughout the experiment. Uniform

* Corresponding author phone: +44 049-8275756; fax: +44 049-8275424; e-mail: andrea.bottacin@unipd.it.
† University of Padova.
‡ University of Vienna and WasserKluster Lunz GmbH.

10.1021/es900852w CCC: $40.75
Published on Web 08/27/2009

flow conditions were obtained by adjusting a tilting weir at the downstream flume end. The resulting flow can be described as shallow rough-bed flow as it is typical in natural headwater streams at base flow. Slopes of the flumes were adjusted to yield identical flume-scale flow velocities but with increasing spatial heterogeneity of flow velocity, roughness, and water depth.

We used sterile unglazed ceramic coupons (1 cm × 2 cm) as a surrogate for natural substratum in biofilm studies (*15, 26*), to determine the areal content of chlorophyll-*a* (*26*). We sampled coupons from triplicate bedforms at the crest, in the trough, upstream, and downstream of the crest at four occasions during biofilm growth. Chlorophyll-*a* served as a surrogate for algal biomass in the highly phototrophic biofilms (*26*). As major building blocks, algae, rather than bacteria, typically conferred the main physical structure to these biofilms. Data were *z*-standardized to remove temporal variability from the primary data induced by biofilm growth, simplify statistical analysis, and to increase statistical power for tests of correlation with bedform height.

Tracer tests were performed with the fluorescent dye Rhodamine-WT (RWT) continuously (30 min) injected upstream using a peristaltic pump with constant flow rate (total injected mass $M = 400$ mg); baffles ensured rapid cross-sectional mixing. Submersible field fluorometers (Turner Designs SCUFA and GGUN-FL20) were used to measure RWT concentration at the flume effluent. RWT may partly adsorb to mineral and organic surfaces, but its sensitivity is greatly superior to halide tracers (e.g., NaCl). In fact, we recovered 98 ± 1% of the RTW in the effluent and did not find any relationship between recovery and bedform height or biofilm development. Therefore, adsorption effects appear negligible. Furthermore, RWT adsorption, seemingly irreversible (*27*) and zero-order (*28*), should not affect the shape of the breakthrough curves.

Solute Transport Modeling

The transport of a conservative solute can be modeled with the following advection−dispersion mass transfer equation:

$$\frac{\partial C(x,t)}{\partial t} + U\frac{\partial C(x,t)}{\partial x} = D\frac{\partial^2 C(x,t)}{\partial x^2} - \alpha\Big(C(x,t) - \int_0^t C(x,t-\tau)\varphi(\tau)\,\mathrm{d}\tau\Big) \quad (1)$$

where $C(x,t)$ is the solute concentration in the surface water [kg m^{-3}], U is the mean flow velocity [m s^{-1}], given by the ratio of the flow rate, and the average flow cross-sectional area $U = Q/A$, D is the longitudinal dispersion coefficient [m^2 s^{-1}], α is a rate of transfer [s^{-1}], and $\varphi(t)$ is the probability density function (PDF) of the residence times in the storage zones [s^{-1}]. It is assumed that the stream reach is uniform, implying that U, D, α, and the PDF $\varphi(t)$ are constant in time and space. Equation 1 is a special case of the STIR model derived from the assumption of Fickian transport in superficial flow (*25*). In the STIR numerical package, the equation is solved by numerical inversion of the analytical solution in the Laplace domain using the De Hoog algorithm (*29*). Essentially, eq 1 is equivalent to the transient storage model (TSM) when $\varphi(t)$ is an exponential distribution, $\varphi(t) = \exp(-t/T)/T$, with mean value T [s] given by $T = A_S/(\alpha A)$, where A_S [m^2] is the cross-sectional area of the transient storage zone.

According to eq 1, the retained mass in a given stream reach of length L can be computed by integrating in space and time the solute fluxes at the stream−storage zone interface:

$$M_S(t) = A\int_0^L \int_0^t \Big(\alpha C(x,t') - \int_0^{t'} \alpha C(x,\tau)\varphi(t'-\tau)\,\mathrm{d}\tau\Big)\,\mathrm{d}t'\,\mathrm{d}x \quad (2)$$

In the Laplace domain, this expression becomes

$$\tilde{M}_S(s) = A\frac{\alpha}{s}(1 - \tilde{\varphi}(s))\int_0^L \tilde{C}(x,s)\,\mathrm{d}x \quad (3)$$

where the symbol (˜) denotes the Laplace transform of the function it is applied to:

$$\tilde{\varphi}(s) = \int_0^\infty \phi(t)\,\mathrm{e}^{-st}\,\mathrm{d}t \quad (4)$$

As shown in Marion et al. (*25*), the residence time distribution (RTD) in a stream segment of length L associated to eq 1 is given by

$$\tilde{r}(s;L) = \tilde{r}_W(s + \alpha(1 - \tilde{\varphi}(s));L) \quad (5)$$

where $\tilde{r}_W$ is the Laplace transform of the RTD in the surface stream in the absence of any storage. In the time domain, this implies the following series expansion:

$$r(t;L) = \sum_{m=0}^{\infty} \int_0^t r_W(\tau;L)\frac{(\alpha\tau)^m}{m!}\,\mathrm{e}^{-\alpha\tau}(\varphi(t-\tau))^{*m}\,\mathrm{d}\tau \quad (6)$$

where $(\varphi(t))^{*m}$ denotes the m-fold convolution of the function $\varphi(t)$ with itself.

Estimating the residence time distribution in the storage zones from a single breakthrough curve is similar to performing a blind deconvolution where also the residence time function in the surface water has to be determined. The problem can be solved by assuming a certain form for the RTD in the storage zones and in the surface water and by determining the relevant parameters by taking the best-fit values in a least-squares sense.

Model Calibration

The effect of biofilm on solute retention has been quantified as follows. The model is fitted to the experimental breakthrough curves relevant to the beds without biofilm. This allows determining the parameters of the surface transport, D and A, and the retention parameters due to solute exchange with the bottom layer of gravel, $\alpha(t_B = 0)$ and $\varphi(t;t_B = 0)$, where t_B is the age of biofilms [days]. Since comparison between the experimental breakthrough curves at subsequent phases of biofilm growth suggests increased retention, the exchange rate and the storage time function are expressed as follows:

$$\begin{aligned} \alpha(t_B) &= \alpha(t_B = 0) + \delta\alpha(t_B) \\ \varphi(t;t_B) &= \frac{1}{\alpha(t_B)}[\alpha(0)\varphi(t;0) + \delta\alpha(t_B)\delta\varphi(t;t_B)] \end{aligned} \quad (7)$$

where $\delta\alpha(t_B)$ and $\delta\varphi(t;t_B)$ represent the increment with respect to the initial configuration (at $t_B = 0$). These additional terms are determined by fixing the parameters of the superficial transport, D and A, and the previously found retention parameters $\alpha(0)$ and $\varphi(t;0)$. The resulting exchange rate and retention function reflect the various effects of biofilms on solute transport. These may include storage in biofilm pores, microeddies around biofilm streamers, and changes in the near-bed flow field and in the related interfacial hydrodynamic exchange. In this sense, the overall statistics of the residence times in the storage zones should not be considered as the result of the sum of the residence times in distinct physical domains.

Determining the parameters of the surface transport and the basic retention for the bed without biofilm, we assumed

that the storage time function can be represented as a normalized sum of two exponential PDF:

$$\varphi(t) = \frac{1}{\alpha}\sum_{i=1}^{2}\frac{\alpha_i}{T_i}\,e^{-t/T_i} \tag{8}$$

where

$$\alpha = \sum_{i=1}^{2}\alpha_i \tag{9}$$

This assumption corresponds to the following conceptualization of the problem. Transport processes acting on time scales of the longitudinal advection due to the mean flow velocity are represented by the advection and dispersion terms and are considered as part of the superficial transport. Processes acting on longer time scales are considered retention processes and are split into fast and long-term retention. The use of two exponential PDF provides good fit of the experimental breakthrough curves, both in linear and log scale. Conversely, if only one exponential PDF is used, as in the TSM, it is not possible to obtain acceptable representation of the tails of the breakthrough curves (Figure S3, Supporting Information). On the other hand, if more than two exponential PDF are used to represent the storage time function, and a lower bound for the corresponding mean residence time is not imposed, a portion of what we identify as superficial transport may become part of the retention processes. Previous studies used an extended version of the TSM to identify two distinct storage zones with exponential residence time distributions (*22, 30*).

A decomposition similar to eqs 8 and 9 is adopted for $\delta\varphi(t;t_B)$, but now an arbitrarily large number of exponential PDF can be used as basis functions. Since the parameters of the superficial transport and of the basic retention are constant, the solution converges to a unique function $\delta\varphi(t;t_B)$ and exchange rate $\delta\alpha(t_B)$ within the time range of the experimental observations.

Model calibration is performed in mixed-scale using a linear scale to fit the bulk of the curve and a log-scale for the tail. More specifically, in the optimization procedure, the following root-mean-square is minimized:

$$\varepsilon = \frac{\sum_{i\in I_U}(C_{sim,i} - C_{obs,i})^2}{\left(\max_{i\in I} C_{obs,i} - \min_{i\in I} C_{obs,i}\right)^2} + \frac{\sum_{i\in I_L}(\log C_{sim,i} - \log C_{obs,i})^2}{\left(\max_{i\in I}(\log C_{obs,i}) - \min_{i\in I}(\log C_{obs,i})\right)^2} \tag{10}$$

where C_{obs} and C_{sim} are the observed and simulated concentration values, respectively, I_U and I_L are the sets of the observed values higher and lower than a given threshold concentration, respectively, and $I = I_U \cup I_L$ is the total set. The threshold value was set equal to 20% of the peak concentration. Particular care was taken in calculating $\min(\log C_{obs,i})$ by neglecting the concentration values closer to zero, generally by excluding from the computation 5% of the total set corresponding to the lowest values. The optimization was performed using the differential evolution method for global optimization by Storn and Price ((*31*), see also ref *32*).

Results and Discussion

Experimental work combined with the STIR model allowed us to investigate the effect of biofilm-induced transient storage as a function of both bed morphology and biofilm age. The breakthrough curve fitting procedure for the initial configuration of the bed with clean gravel ($t_B = 0$) shows that both exchange rates, α_1 and α_2, and the mean residence times in the storage zones, T_1 and T_2, are characterized by variations between the flumes up to 20% of their respective mean value; however, no particular trend was observed (Table 1, Figure S3 in the Supporting Information). A detailed analysis of the behavior of these parameters shows that when transfer rates are lower, the average residence times tend to increase. We tentatively attribute this behavior to flow irregularities and will further investigate this relationship. Only adequately long residence times are represented by the storage term in the model, while retention processes acting on small time scales are represented as part of the surface flow field and affect the longitudinal dispersion coefficient. The long-term retention is expected to be associated with the bottom layer of gravel, which had similar characteristics for all the flumes. However, the physically constrained gravel layer prevents deeper exchange into the bed as expected from bedform-induced pumping (*2, 3*). However, the storage effect due to flow detachment and to the formation of a local eddy with low velocities downstream of the bedform constitutes a retention process acting on the same time scale as the superficial advection and dispersion processes. Since flow is characterized by low submergence, the increase in bedform height affects the whole surface flow field by increasing its heterogeneity (i.e., the velocity variance), which can be represented by an enhanced dispersion coefficient. The coefficient D is almost 60% higher with bedforms of $H = 10$ cm than of $H = 2$ cm (Table 1), and there is a clear increasing trend for the intermediate flumes. The flow cross-sectional area, A, as well as the average velocity, $U = Q/A$, where $Q = 2.25\ L\ s^{-1}$, are almost constant for all the flumes, with a slightly increasing trend with bedform height. This increase is limited to 10% of the mean value, which is equal to $A = 0.028\ m^2$ and corresponds to an average flow depth $d = 7$ cm.

Once the parameters for the superficial flow field and the basic retention for the beds without biofilms are determined, the additional retention parameters $\delta\alpha$ and $\delta\varphi(t)$ are estimated for the biofilm ages $t_B = 8$, 18, 26, 32 days while holding the former fixed. The simulated concentration curves (Figure S3, Supporting Information) were obtained by decomposing the additional retention function, $\delta\varphi(t)$ into three exponential PDF according to eqs 8 and 9. No further improvement of the data fitting was observed with an

TABLE 1. Estimated Parameters of the STIR Model for Beds without Biofilm ($t_B = 0$)

H (cm)	2	4	6	8	10
A (m^2)	0.027	0.027	0.027	0.028	0.030
U ($m\ s^{-1}$)	0.083	0.083	0.083	0.080	0.075
D ($m^2\ s^{-1}$)	0.019	0.019	0.020	0.028	0.030
α_1 (s^{-1})	3.74×10^{-4}	3.33×10^{-4}	3.73×10^{-4}	3.58×10^{-4}	3.40×10^{-4}
T_1 (s)	112	121	100	107	118
α_2 (s^{-1})	4.19×10^{-5}	3.63×10^{-5}	4.61×10^{-5}	4.55×10^{-5}	3.80×10^{-5}
T_2 (s)	667	650	603	615	660

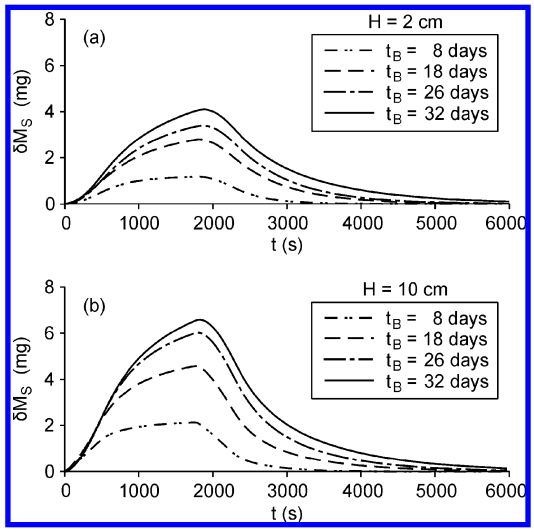

FIGURE 1. Plots of the increment of retained mass, $\delta M_S(t;t_B,H) = M_S(t;t_B,H) - M_S(t;t_B = 0,H)$, versus time, t, for different biofilm ages, t_B, and bedform height H = (a) 2 and (b) 10 cm.

increased number of basis functions. Biofilm effects on solute retention were isolated from a comparison of results from different biofilm growth stages and by calculating the stored mass associated to the exchange parameters derived from model calibration. Figure 1 shows the temporal behavior of the biofilm-induced increment of retained mass δM_S [mg] relative to the initial configuration without biofilm ($t_B = 0$) for $H = 2$ and 10 cm. Plots of δM_S for every flume are shown in Figure S4 in the Supporting Information. δM_S has an increasing trend until the tracer addition stops, and it would theoretically continue asymptotically in the case of a constant continuous injection. The subsequent decrease is due to the advective transport outside the physical domain following gradual release from the retention volumes. Transient storage clearly increases monotonically with biofilm growth over the whole time span of a tracer test, as the curve of stored mass corresponding to a given time t_B (i.e., biofilm age) is always located above the curves from previous time points. The trend of peak values of the stored mass indicates that solute retention increases with biofilm age with a decreasing rate. In fact, it is also expected to asymptotically reach a limit value when the stationary phase of biofilm growth (and constant biofilm thickness) is reached as a balance between factors such as the transfer of nutrients, conversion rates, and detachment forces (steady state equilibrium).

Comparison of the initial temporal trend of the retained mass between the different flumes (Figure 1) suggests an effect of bed morphology on biofilm storage (i.e., increasing mass transfer from $H = 2$ cm to $H = 10$ cm). The peak values of the biofilm-induced increment of retained mass, $\delta M_{S,max}$, are significantly and positively related to bedform height for all biofilms older than 8 days (Figure 2), and the slope of this relationship depends on biofilm age (coefficient of determination $R^2 = 0.90$, probability $P < 0.05$, $n = 5$) and on average chlorophyll-a ($R^2 = 0.97$, $P < 0.05$, $n = 4$). Similarly, slightly weaker relationships can be found for $M_{S,max}$, the peak values of the total retained mass which include the basic retention for $t_B = 0$ (Figure 2). This clearly shows an effect of bedform height on the ability of biofilms to create additional retention zones and further suggests that this effect becomes stronger with biofilm age and biomass. This could be due to enhanced biofilm growth in flumes with higher bedforms which would lead to increasingly diverging biomass among flumes over time and could explain the trends of $\delta M_{S,max}$ and $M_{S,max}$. Indeed, when the observed z_{Chla} values are plotted against bedform height (Figure 3), an increasing trend is suggested ($R^2 = 0.71$, $P < 0.07$), indicating that bed topography may

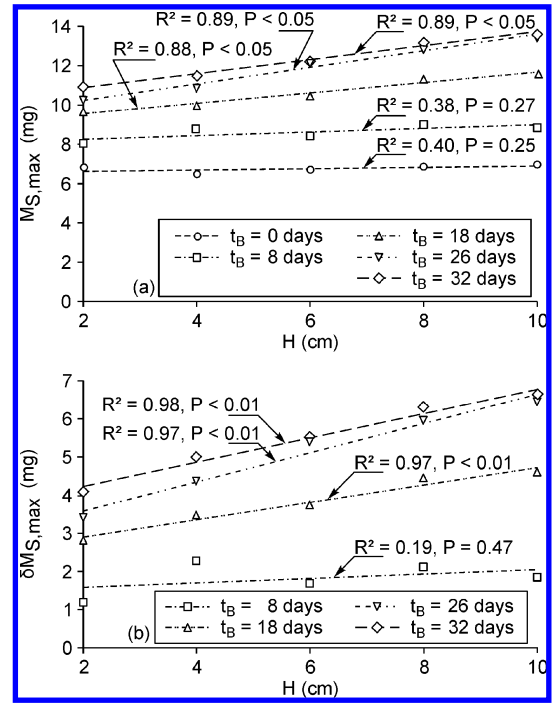

FIGURE 2. (a) Plots of the maximum values of retained mass, $M_{S,max}(t;t_B,H)$ and (b) of the increment of retained mass $\delta M_{S,max}(t;t_B,H)$ versus bedform height, H, for different biofilm ages, t_B. The quantity $M_{S,max}$ includes the effect of the basic retention in the absence of biofilm, which is subtracted to get $\delta M_{S,max}$.

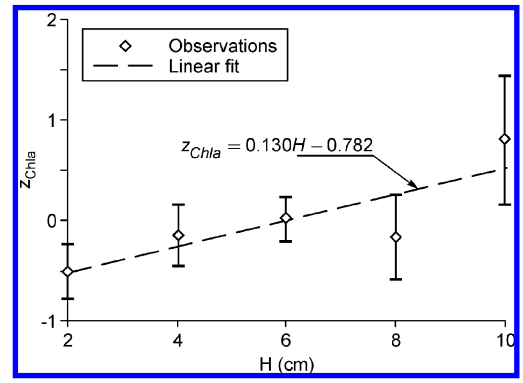

FIGURE 3. Average chlorophyll-a versus bedform height. Since chlorophyll-a increases markedly during biofilm growth, data from four sampling dates were z-standardized within each date to remove temporal variation before averaging and comparison of flumes. Error bars represent 95% confidence intervals.

influence the dynamics of biofilm growth leading to a higher overall biomass in environments with higher heterogeneity. An explanation for this behavior lies in the increased velocity variance associated with a higher variability of bed elevation and generating more turbulent flow fields, which in turn ameliorate nutrient transfer. On the other hand, if detachment is limiting biofilm differentiation, the observed behavior may be due to the downstream shift of the flow reattachment point for higher bedforms implying an extended zone of low shear stress. This effect may exceed the increase of shear stress downstream of the reattachment point up to the crest and induce an overall reduction of the biofilm detachment rate.

Biofilm biomass (chlorophyll-a) explains a large fraction of the variance of biofilm-induced transient storage $\delta M_{S,max}$ (Figure 4), even though a secondary effect of bedform height on $\delta M_{S,max}$ is still visible. A multiple linear regression model with $\delta M_{S,max}$ as the dependent variable and chlorophyll-a

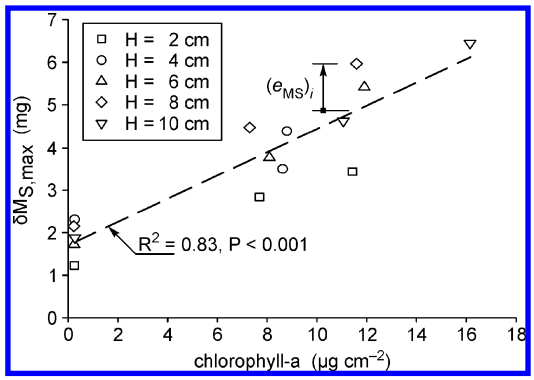

FIGURE 4. Plots of the maximum values of the additional retained mass due to biofilm, $\delta M_{S,max}$, versus chlorophyll-*a*, Chla. The positive slope of the linear regression indicates a positive correlation between transient storage and biomass.

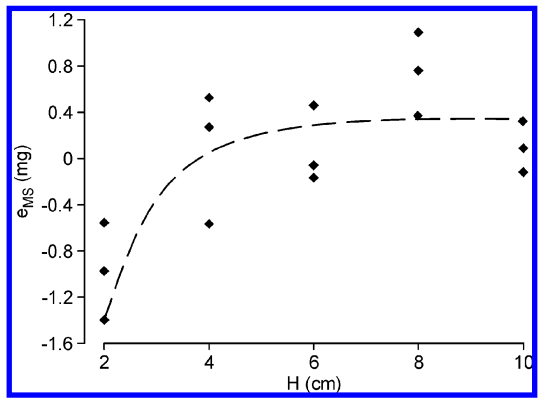

FIGURE 5. Residuals from a linear model explaining $\delta M_{S,max}$ as a function of chlorophyll-*a*, indicated by e_{MS}, can be regarded as descriptors of an effect of biofilm mediated by the bedform that may be attributable to biofilm architecture. Residuals show a saturating trend with bedform height, as suggested by a data fit to an exponential rise to maximum (broken line).

and bedform height as independents identifies significant influences of both predictors ($P < 0.001$ for chlorophyll-*a*, $P < 0.05$ for bedform height, *F*-value $F_{2,12} = 52.2$, overall $P < 0.001$, adjusted $R^2 = 0.88$). Thus, higher bedforms allow biofilms with the same chlorophyll-*a* content to increase their retention capacity.

Residuals from a linear model explaining the biofilm-induced increment of retained mass ($\delta M_{S,max}$) as a function of chlorophyll-*a* (indicated by e_{MS}, Figure 4) can be regarded as a descriptor of an effect of biofilm mediated by the bedform. In fact, when plotted against bedform height (Figure 5), a curvilinear relationship becomes evident, suggesting saturation with increasing bedform height. Apart from increased penetration efficiency due to bedform-associated turbulence, this behavior may be attributable to complex interactions between biofilm architecture and near-bed flow. Indeed biofilms developed different architectures in relation to the different bed morphology and hydrodynamic conditions. Biofilms developed directed architectures with filamentous streamers at exposed microhabitats (bedform crests), while biofilm growing in quiescent zones between bedforms largely consisted of nondirected coalescing microcolonies. These patterns were pronounced in flumes with higher bedforms and induced turbulence (*26*). Thus, biofilms are expected to increase transient storage not only via a biomass effect, but also by the formation of an explicit spatial architecture, developed as an adaptation to local hydrodynamic conditions. Indeed, biofilm architecture can be regarded as a remarkable adaptation to optimize solute (i.e., nutrient and energy substrate) replenishment in a given hydrodynamic environment (*15*) and could thus also explain the overall increase of biomass with bedform height. Thus, higher retention would result from biofilm structural differentiation, which in turn favors biofilm growth and further increases the retention volume.

Overall, the transient storage induced by the biofilm is sizable compared to the storage in the porous bed, as $M_{S,max}$ reaches values varying from 150% to around 200% of the initial retention $M_S(t_B = 0)$ for $H = 2$ and 10 cm, respectively (Figure 2). This is valid at least in this particular case in which the depth of the sediment layer is limited as in constrained hyporheic zones (*23*). While benthic biofilms can clog the underlying sediments and thereby reduce solute penetration, streamers may increase turbulent mass transfer, which is a complex fluid-structure interaction problem that remains largely unexplored.

Acknowledgments

The experiments were funded by the Austrian Science Foundation (FWF), the European Science Foundation (EuroDIVERSITY, COMIX), and the Land Niederösterreich to T.J.B.. The participation of Andrea Bottacin-Busolin and Andrea Marion was funded by the "Ateneo Project" of the University of Padova "Hyporheic Transport in Rivers". The authors thank Iris Hödl, Katharina Besemer, and Tommaso Musner for assistance with the flumes and in the laboratory.

Note Added after ASAP Publication

This article was released ASAP on August 27, 2009, with minor errors in the text. The correct version was posted September 2, 2009.

Supporting Information Available

Longitudinal sketch of a bedform, pictures of the gravel with and without biofilms, graphs of the experimental and simulated breakthrough curves and of the increment of retained mass versus time at different biofilm ages. This material is available free of charge via the Internet at http://pubs.acs.org.

Literature Cited

(1) Thibodeaux, L. J.; Boyle, J. D. Bedform-generated convective transport in bottom sediment. *Nature* **1987**, *325*, 341–343.
(2) Elliott, A. H.; Brooks, N. H. Transfer of nonsorbing solutes to a streambed with bed forms: Theory. *Water Resour. Res.* **1997**, *33* (1), 123–136.
(3) Elliott, A. H.; Brooks, N. H. Transfer of nonsorbing solutes to a streambed with bed forms: Laboratory experiments. *Water Resour. Res.* **1997**, *33* (1), 137–151.
(4) Marion, A.; Bellinello, M.; Guymer, I.; Packman, A. Effect of bed form geometry on the penetration of nonreactive solutes into a streambed. *Water Resour. Res.* **2002**, *38* (10), 1209.
(5) Marion, A.; Zaramella, M. Diffusive behavior of bedform-induced hyporheic exchange in rivers. *J. Environ. Eng.* **2005**, *131* (9), 1260–1266.
(6) Packman, A. I.; Mashfiqus, S.; Zaramella, M. Hyporheic exchange with gravel beds: Basic hydrodynamic interactions and bedform-induced advective flows. *J. Hydraul. Eng.* **2004**, *130* (7), 647–656.
(7) Salehin, M.; Packman, A. I.; Paradis, M. Hyporheic exchange with heterogeneous streambeds: Laboratory experiments and modeling. *Water Resour. Res.* **2004**, *40*, W11504.
(8) Marion, A.; Packman, A. I.; Zaramella, M.; Bottacin-Busolin, A. Hyporheic flows in stratified beds. *Water Resour. Res.* **2008**, *44*, W09433.
(9) Harvey, J. W.; Bencala, K. V. The effect of streambed topography on surface-subsurface water exchange in mountain catchments. *Water Resour. Res.* **1993**, *29* (1), 89–98.
(10) Boano, F.; Camporeale, C.; Revelli, R.; Ridolfi, L. Sinuosity-driven hyporheic exchange in meandering rivers. *Geophys. Res. Lett.* **2006**, *33*, L18406.
(11) Cardenas, M. B. The effect of river bend morphology on flow and timescales of surface water-groundwater exchange across pointbars. *J. Hydrol.* **2008**, *362* (1−2), 134–141.

(12) Sigee, D. C. *Freshwater Microbiology*; Wiley: Chichester, U.K., 2005.
(13) Battin, T. J.; Kaplan, L. A.; Findlay, S.; Hopkinson, C. S.; Marti, E.; Packman, A. I.; Newbold, J. D.; Sabater, F. Biophysical controls on organic carbon fluxes in fluvial networks. *Nat. Geosci.* **2008**, *1* (2), 95–100.
(14) Mulholland, P. J.; Helton, A. M.; Poole, G. C.; Hall, R. O.; Hamilton, S. K.; Peterson, B. J.; Tank, J. L.; Ashkenas, L. R.; Cooper, L. W.; Dahm, C. N. Stream denitrification across biomes and its response to anthropogenic nitrate loading. *Nature* **2008**, *452* (7184), 202–205.
(15) Battin, T. J.; Kaplan, L. A.; Denis Newbold, J.; Hansen, C. M. E. Contributions of microbial biofilms to ecosystem processes in stream mesocosms. *Nature* **2003**, *426* (6965), 439–442.
(16) Kim, B. K.; Packman, A. I.; Triska, F. J. Modeling transient storage and nitrate uptake kinetics in a flume containing a natural periphyton community. *Water Resour. Res.* **1990**, *26* (3), 505–515.
(17) Kim, B. K. A.; Jackman, A. P.; Triska, F. J. Modeling biotic uptake by periphyton and transient hyporrheic storage of nitrate in a natural stream. *Water Resour. Res.* **1992**, *28* (10), 2743–2752.
(18) Bencala, K. E. Interactions of solutes and streambed sediment 2. A Dynamic analysis of coupled hydrologic and chemical processes that determine solute transport. *Water Resour. Res.* **1984**, *20* (12), 1804–1814.
(19) Mulholland, P. J.; Steinman, A. D.; Marzolf, E. R.; Hart, D. R.; DeAngelis, D. L. Effect of periphyton biomass on hydraulic characteristics and nutrient cycling in streams. *Oecologia* **1994**, *98* (1), 40–47.
(20) DeAngelis, D. L.; Loreau, M.; Neergaard, D.; Mulholland, P. J.; Marzolf, E. R. Modelling nutrient-periphyton dynamics in streams: the importance of transient storage zones. *Ecol. Model.* **1995**, *80* (2−3), 149–160.
(21) Dent, C. L.; Henry, J. C. Modelling nutrient-periphyton dynamics in streams with surface-subsurface exchange. *Ecol. Model.* **1999**, *122* (1−2), 97–116.
(22) Gooseff, M. N.; McKnight, D. M.; Runkel, R. L.; Duff, J. H. Denitrification and hydrologic transient storage in a glacial meltwater stream, McMurdo Dry Valleys, Antarctica. *Limnol. Oceanogr.* **2004**, *49* (5), 1884–1895.
(23) Orr, C. H.; Clark, J. J.; Wilcock, P. R.; Finlay, J. C.; Doyle, M. W. Comparison of morphological and biological control of exchange with storage zones in a field-scale flume. *J. Geophys. Res. Lett.* **2009**, *114*, G02019.
(24) Marion, A.; Zaramella, M. A residence time model for stream-subsurface exchange of contaminants. *Acta Geophys. Pol.* **2005**, *53* (4), 527.
(25) Marion, A.; Zaramella, M.; Bottacin-Busolin, A. Solute transport in rivers with multiple storage zones: The STIR model. *Water Resour. Res.* **2008**, *44*, W10406.
(26) Besemer, K.; Singer, G.; Limberger, R.; Chlup, A.; Hochedlinger, G.; Hodl, I.; Baranyi, C.; Battin, T. J. Biophysical controls on community succession in stream biofilms. *Appl. Environ. Microbiol.* **2007**, *73* (15), 4966–4974.
(27) Smart, P. L.; Laidlaw, I. M. S. An evaluation of some fluorescent dyes for water tracing. *Water Resour. Res.* **1977**, *13*, 15–33.
(28) Dierberg, F. E.; DeBusk, T. A. An evaluation of two tracers in suface-flow wetlands: Rhodamine-WT and lithium. *Wetlands* **2005**, *25* (1), 8–25.
(29) De Hoog, F. R. An improved method for numerical inversion of Laplace transforms. *SIAM J. Sci. Stat. Comput.* **1982**, *3* (3), 357–366.
(30) Harvey, J. W.; Saiers, J. E.; Newlin, J. T. Solute tranposrt and storage mechanisms in wetlands of the Everglades, south Florida. *Water Resour. Res.* **2005**, *41*, W05009.
(31) Storn, R.; Price, K. Differential evolution−A simple and efficient heuristic for global optimization over continuous spaces. *J. Global Optim.* **1997**, *11*, 341–359.
(32) Price, K. V.; Storn, R. M.; Lampinen, J. A. *Differential Evolution*; Natural Computing Series; Springer: Berlin, Germany, 2005.

ES900852W